Analysis of natural convection melting from a heated wall with vertically oriented fins

M. Lacroix and M. Benmadda

Département de génie mécanique, Université de Sherbrooke, Sherbrooke, Canada

Received July 1996
Revised April 1997
Accepted June 1997

Nomenclature

a,b	Constants in correlation and source term in equation 5
B	Parameter [$=(1-f_L)\times 10^{15}$]
C_k	Phase-specific heat
f_L	Local liquid fraction
g	Acceleration of gravity ($m.s^{-2}$)
h	Sensible volumetric enthalpy
H	Height of the cavity (m)
$H(T)$	Total volumetric enthalpy
k	Thermal conductivity ($W.m^{-1}.°C^{-1}$)
L	Length of fin (m)
L_F	Latent heat ($J.kg^{-1}$)
MVF	Molten volume fraction
n	Normal direction to the surface
Nu_H	Average Nusselt number at the wall
p	Pressure
PCM	Phase change material
Ra_H	Rayleigh number $\left(=\frac{g\beta(T_H - T_m)H^3}{\upsilon\alpha}\right)$
S	Total surface of the wall and fins (m^2/m)
$S_\phi(x, y)$	Source term in equation 1
t	Time (s)
T	Temperature (K)
u	Horizontal component of the velocity ($m.s^{-1}$)
v	Vertical component of the velocity ($m.s^{-1}$)
W	Width of the cavity (m)
x, y	Space variables
α	Thermal diffusivity ($m^2.s^{-1}$)
β	Thermal expansion coefficient (K^{-1})
Γ_ϕ	Exchange coefficient
ν	Kinematic viscosity ($m^2.s^{-1}$)
μ_L	Dynamic viscosity ($\upsilon\rho$)
ρ	Density ($kg.m^{-3}$)
ϕ	General dependent variable
ω	Relaxation parameter

Superscripts

$i, i+1$	Iteration
OLD	Previous time step

Subscripts

H	Heated wall
L	Melt
m	melting point
N, S, W, E, P	Nodal locations

Introduction

A major drawback of phase change materials (PCMs) commonly used in latent heat thermal energy storage systems is their low thermal conductivity (~0.2W/mK) which prevents rapid transfer of heat during heat storage (melting) and heat recovery (solidification). One way to alleviate this problem is to embed fins in the PCM, attached to the heat transfer surface, so that the total heat transfer area is increased.

The authors are very grateful to the Natural Science and Engineering Council of Canada, to the Ministère des Ressources Naturelles du Québec and to the Canadian Agency for International Development for their financial support.

International Journal of Numerical Methods for Heat & Fluid Flow
Vol. 8 No. 4, 1998, pp. 465–478.

Few studies on the utilization of fins embedded in PCMs have been reported in the open literature (Eftekhar *et al.,* 1984; Padmanabhan and Murthy, 1986; Sasaguchi, 1989; Sasaguchi *et al.,* 1988). Sasaguchi and coworkers (Sasaguchi *et al.,* 1988) conducted an experimental and theoretical study on the effects of the configuration of a finned tube on the heat transfer characteristics of a latent heat thermal energy storage unit. Sasaguchi (1989) later carried out a three-dimensional numerical calculation to predict the performance of a longitudinal finned-tube latent heat storage unit. The effects of the NTU and Biot numbers on the heat transfer process were examined. Padmanabhan and Murthy (1986) presented a theoretical analysis for the transient, solid-liquid phase change process occurring in a cylindrical annulus in which rectangular circumferential fins are attached to the inner tube. Eftekhar and his colleagues (Eftekhar *et al.,* 1984) reported an experimental study of the heat transfer enhancement in a paraffin wax thermal storage system consisting of vertically arranged fins between a heated and a cooled horizontal finned-tube arrangement.

In order to focus on the overall thermal performance of the systems, all the aforementioned studies rest on the simplifying assumption that conduction is the sole mechanism of heat transfer through the PCM. Convection heat transfer in the melt is neglected. As a result, these models cannot predict accurately the melting rates nor track the complex motion of the solid-liquid interfaces.

Recently, Sasaguchi and Takeo (1994) conducted a numerical analysis of convection dominated melting in porous media around a hot surface with conducting fins. The effect of the orientation of the hot surface on the effectiveness of the attached fins was examined. It was found that the melting rate is the largest for the melting from below and the smallest for the melting from above.

The objective of the present paper is to study the effect of vertically oriented fins embedded in the PCM on the melting process. The fins are either attached to the top heated wall or to the bottom heated wall of a rectangular cavity made of two large parallel plates. The number of fins per meter and the magnitude of the Rayleigh number are examined. A computational methodology is first presented for handling the complex problem of natural convection dominated melting from a finned wall. The model is next validated with experimental data and the results of a parametric study are then presented and discussed.

Physical model

The physical system considered in the present study is shown in Figure 1. An insulated rectangular cavity made of two parallel plates separated by a distance H is filled with the PCM. Vertical rectangular fins of length L and thickness δ emerge from the top (case A) or the bottom (case B) plate. The distance between the fins is W. The dimensions of the parallel plates are assumed to be much larger than the gap space H and, as a result of the symmetry of the problem, a simplified two-dimensional analysis, as shown in Figure 1, can be applied. At times $t = 0$, the PCM is solid and its temperature is uniform, constant and below

the melting point T_m. At time t = 0, the temperature of the finned wall is impulsively raised to a prescribed temperature T_H above the fusion point. Consequently, heat is quickly conducted across the fins and slowly conducted through the PCM and melting is eventually triggered.

It is assumed in the analysis that the thermophysical properties of the PCM are temperature independent but may be different for the liquid and solid phases. The Boussinesq approximation is valid for the liquid density variations in the buoyancy source term. The liquid phase is Newtonian and the fluid motion in the melt is laminar. Viscous dissipation is neglected.

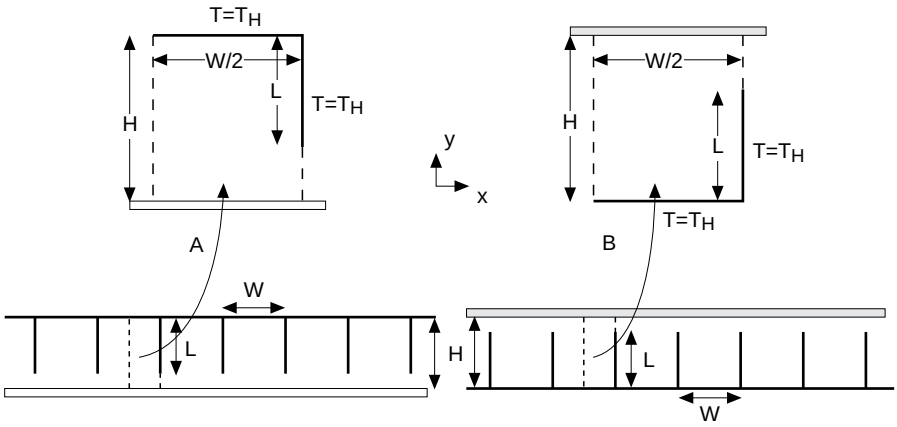

Figure 1. Schematic representation of the enclosure and symmetry of the problem

Subjected to the foregoing assumptions, the governing equations for the conservation of mass, momentum and energy are expressed in terms of a general transport equation for the property ϕ:

$$\frac{\partial}{\partial t}(\rho\phi) + \frac{\partial}{\partial x}(\rho u\phi - \Gamma_\phi \frac{\partial \phi}{\partial x}) + \frac{\partial}{\partial y}(\rho v\phi - \Gamma_\phi \frac{\partial \phi}{\partial y}) = S_\phi(x,y) \quad (1)$$

$S_\phi(x,y)$ is a source term, Γ_ϕ is an exchange coefficient and ρ is the density. These parameters and properties are defined in Table I.

Equation	ϕ	ρ	Γ_ϕ	$\mathbf{S_\phi(x,y)}$
Mass	$\vec{V}$	ρ	0	0
Momentum x	u	ρ	μ_L	$-\frac{\partial p}{\partial x} + S_u$
Momentum y	v	ρ	μ_L	$-\frac{\partial p}{\partial y} - \rho_0 g\beta(T - T_m) + S_v$
Energy	h	ρ	$\frac{k}{c_p}$	$S_h = -\rho L_F \frac{\partial f_L}{\partial t}$

Table I. Parameters and properties in equation (1)

The enthalpy equation follows Crank's (1984) formulation for which the total enthalpy is split into sensible and latent heat components:

$$H(T)=h(T)+\rho_s L_f f_L$$

$$h(T) = \int_{T_m}^{T} \rho_k C_k L_F f_L$$

and ρ_k is the phase density, C_k is the phase-specific heat, T_m is the phase change temperature and f_L is the local liquid fraction. The potential advantage of this formulation is that the enthalpy equation is cast in a standard form and the problems associated with the phase change are isolated in a source term S_h. The source terms S_u and S_v in the momentum equations are defined as

$$S_u = Bu \qquad \text{and} \qquad S_v = Bv$$

where the parameter B is taken as a function of local liquid fraction such that $B = (1-f_L) \times 10^{15}$.

Hence, the liquid fraction is used to drive the velocity components to zero in the solid phase of the PCM via the source terms S_u and S_v ($f_L = 0$ and $B = 10^{15}$; as a result, $u = v = 0$). Conduction across the fins is also taken into account by setting the velocity components u and v to zero in the energy conservation equation (1).

The boundary conditions for the conservation equations are:
at the heated wall and,

$$T=T_{H,,} \qquad u=v=0 \tag{2}$$

at the horizontal adiabatic wall,

$$\frac{\partial T}{\partial y} = 0,, \qquad u=v=0 \tag{3}$$

and at the symmetric vertical planes,

$$\frac{\partial T}{\partial x} = 0, \frac{\partial u}{\partial x} = 0, \frac{\partial v}{\partial x} = 0 \tag{4}$$

Numerical procedure

The finite difference equations are obtained on integrating the general governing equation, equation (1), over each of the control volumes in the (x,y) plane. The resulting finite difference scheme has the form

$$A_P\phi_P = A_E\phi_E + A_S\phi_S + A_W\phi_W + A_N\phi_N + b \tag{5}$$

Expressions for the coefficients in equation (5) may be found in Benmadda (1996). The advection-diffusion part of coefficient A_S,A_W,A_P,A_E and A_N is modified for stability according to the power law scheme of Patankar (1980). b is the source term S and it includes the value ϕ_P from the previous time step.

The SIMPLEC algorithm is adopted to solve the velocity-pressure coupling of equation (5) (Van Doormaal and Raithby, 1984).

The central feature of the present enthalpy fixed grid technique is the source term b for the enthalpy equation, i.e.,

$$b = \rho L_F \left[f_L^{OLD} - f_L^i \right] \frac{\Delta x \Delta y}{\Delta t} + \rho \frac{\Delta x \Delta y}{\Delta t} h_P^{OLD} \tag{6}$$

The first term on the right hand-side of equation (6) keeps track of the latent heat evolution, and its driving element is the local liquid fraction f_L. This fraction takes the values of 1 in fully liquid regions, 0 in fully solid regions, and lies in the interval [0,1] in the vicinity of the phase front. In a numerical implementation its value is determined iteratively from the solution of the enthalpy equation. Hence, after the (i + 1) th numerical solution of the enthalpy equation over the entire computational domain, equation (5) may be written as

$$A_P h_P = A_E h_E + A_S h_S + A_W h_W + A_N h_N + \rho L_F \left[f_L^{OLD} - f_L^i \right] \frac{\Delta x \Delta y}{\Delta t} + \rho \frac{\Delta x \Delta y}{\Delta t} h_P^{OLD} \tag{7}$$

If the phase change is occurring about the Pth node, i.e. $0 < f_L < 1$, then the ith estimate of the liquid fraction needs to be updated such that left-hand side of equation (7) is zero; that is

$$A_P h_P = A_E h_E + A_S h_S + A_W h_W + A_N h_N + \rho L_F \left[f_L^{OLD} - f_L^i \right] \frac{\Delta x \Delta y}{\Delta t} + \rho \frac{\Delta x \Delta y}{\Delta t} h_P^{OLD} \tag{8}$$

Subtracting equation (8) from equation (7) yields the following update for the liquid fraction at nodes where the phase change is taking place:

$$f_L^{i+1} = f_L^i + \omega \frac{\Delta t}{\Delta x \Delta y \rho L_F} A_P h_P \tag{9}$$

where ω is a relaxation parameter. The liquid fraction update is applied at every node after the ith solution of the linear system, equation (5), for h. To account for the fact that equation (9) is not appropriate at every node, the overshoot/ undershoot correction,

$$f_L = 0 \quad \text{if} \quad f_L^{i+1} \le 0$$

$$f_L = 1 \quad \text{if} \quad f_L^{i+1} \ge 1$$

is used immediately after equation (9). The iterative solution continues until convergence of the flow and energy fields at every time step. Convergence is declared when the largest residual for all difference equations is smaller than 10^{-3} . More stringent convergence criteria were retained but the results did not show noticeable changes in the solutions. Further details on the numerical

procedure and its implementation are provided in Benmadda (1996); Brent *et al.* (1988); Lacroix and Benmadda (1997).

Model validation

The foregoing computational model was first validated for transient natural convection from a finned surface for thermal storage in enclosures. These results are reported by Benmadda and Lacroix (1996) and need not be repeated here. The model was also validated with experimental data for natural convection dominated melting of *n*-octadecane from a finned wall. An experimental storage unit was constructed and experiments were performed for a heated vertical wall with horizontal fins. The solid-liquid profiles were photographed with a camera and the area of the unmelted solid PCM was thus evaluated yielding the temporal variation of the molten volume fraction.

As an example, a comparison between the experimentally determined and predicted melting front profiles at different times is provided in Figure 2. The experimental profiles were hand drawn by superposing the output plots of the numerical simulation to the pictures taken from the camera. In this case, five equally spaced horizontal fins are attached to the vertical right wall which is maintained at an average temperature of T_H = 333K. The corresponding Rayleigh number based on the height of the cavity is $Ra = 4.2 \times 10^9$. The numerical simulation was carried out with a grid size of 60×100 non-uniformly distributed control volumes and a constant time step of 60*s*. Calculations

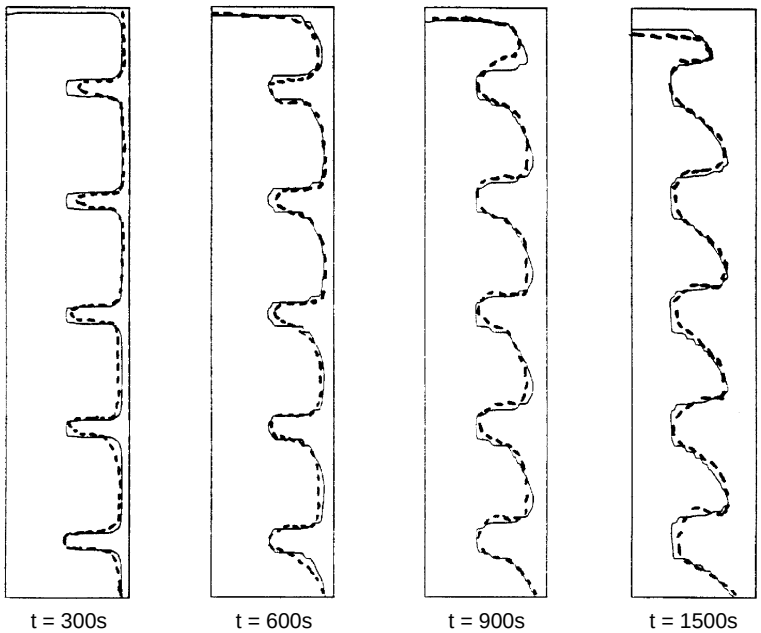

Figure 2.
Comparison of predicted melting front positions with experimental contours
(—: predictions;
----: experiment)

performed with finer grids (70×120) and shorter time steps (30*s*) did not show perceptible differences in the predicted melting front profiles.

Figure 2 reveals that the numerical predictions are in very good agreement with the experimental data. Factors responsible for the small discrepancy between measured and predicted interface positions are the initial contamination of the PCM with trapped air bubbles (the PCM was purposely not degasified before the experiment) and the difficulties of maintaining a constant and uniform temperature over the entire surface of the heated wall in the course of the experiment (~4 hours). Moreover, the model does not take into account the volume expansion due to the phase change from the solid to the liquid, nor the temperature-dependent thermophysical properties, the surface tension effects at the top of the melt and the non-Newtonian behavior of the liquid near the solid-liquid interface.

The predicted instantaneous molten volume fraction, MVF, was evaluated from the solid-liquid interface by a numerical integration of the instantaneous measured position. In a simulation, the molten volume fraction is estimated at a time *t* via the integral of the local liquid fractions over the entire volume occupied by the PCM:

$$\mathrm{MVF}(t) = \frac{2}{H \cdot W} \sum_{i,j} f_L\left(x_i, y_j, t\right) \cdot \Delta x_i \Delta y_j$$

A comparison of the experimental data with the predicted molten volume fractions is shown in Figure 3. These results are for a heated wall with no fin, one fin and five fins, maintained at temperatures ranging from 313K ($Ra = 1.5 \times 10^9$) to 333 K ($Ra = 4.2 \times 10^9$). It is apparent from this figure that the agreement is excellent. Further details on the experimental set-up and the

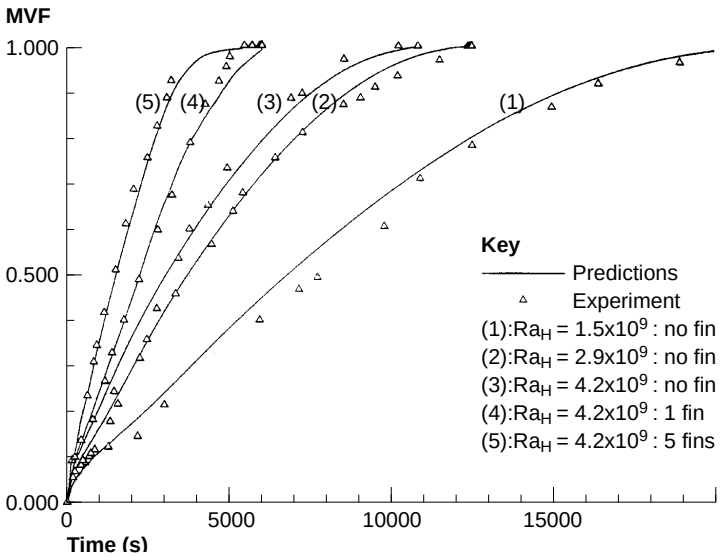

Figure 3.
Comparison of predicted and experimentally determined molten volume fractions

validation of the model may be found in Benmadda (1996); Lacroix and Benmadda (1997).

Results and discussion

A series of numerical simulations were conducted to study the effect of long vertical rectangular fins attached to the top or to the bottom wall of a narrow horizontal cavity (H = 2cm) on the melting process. The phase change material is n-octadecane. The fin size ratio L/H was maintained at 0.75. Shorter fins were not considered here since it was found in a recent study that the effect of their number on the melting process is negligible (Lacroix and Benmadda, 1997). The distance W between the fins varied from 0.6cm to 2cm (166 fins/m down to 50 fins/m). Results were obtained for temperatures of the heated finned wall ranging from 13K to 53K above the melting point of *n*-octadecane (T_m~300K) i.e. for $2.10 \times 10^6 \leq Ra_H \leq 8.57 \times 10^6$. To ensure grid independence, grid studies were performed at the highest Rayleigh number where the velocity and thermal boundary layers are thinnest. By increasing the grid size for the microcavity shown in Figure 1 from 21×31 to 41×61, the average Nusselt number at the heated surfaces changed by at most 1.5 percent. Moreover, the effect of the grid sizes employed in the present study on the predicted melting front profiles was hardly perceptible. The computations were conducted on an IBM RISC-6000 work station model 375. The longest simulation carried out required 30 CPU minutes.

Figure 4 shows the time evolution of the predicted temperature distributions between fins attached to the top heated wall (case A) and attached to the bottom heated wall (case B) respectively. In both cases, W = 0.75cm and $Ra_H = 8.57 \times 10^6$. It is evident from these figures that the melting process for case A (top heating) is slower than that for case B (bottom heating). Conduction dominated melting prevails for a longer period of time in case A (the isotherms appear to be uniformly parallel to the heated surfaces) and when buoyancy driven flows are triggered in the melt, they remain relatively weak. On the other hand, for case B, part of the heat is transferred through the melt from the bottom heated wall to the top cold phase front. This situation is unstable as layers of cold denser fluid adjacent to the solid-liquid interface lie above layers of hot and lighter fluid near the bottom heated wall. As a result, complex recirculating flows are eventually triggered at the bottom heated wall and near the top of the fin (t = 600s) thereby increasing significantly the melting rate in these regions.

The overall effect of the position of the fins and of the Rayleigh number on the temporal variation of the molten volume fraction is exemplified in Figure 5. These figures clearly show that the melting rates are larger for bottom finned heated walls and for increasing Rayleigh number. Indeed, for $Ra_H = 8.57 \times 10^6$, melting from the top finned wall takes approximately 2000s to be completed while melting from the bottom finned wall requires only 1000s.

Figure 6 elucidates the corresponding temporal variation of the average Nusselt number Nu_H at the heated surfaces. This number was evaluated from the temperature distribution in the melt as

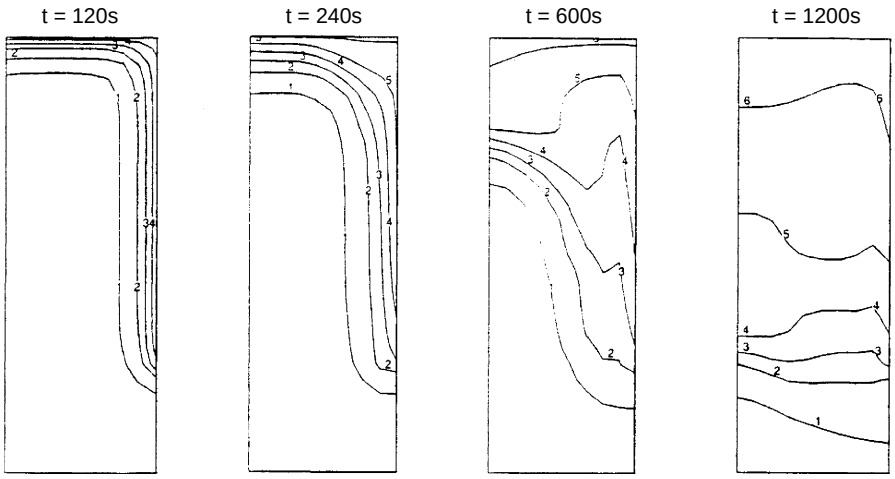

Figure 4a.
Isotherm map for top heating (case A)

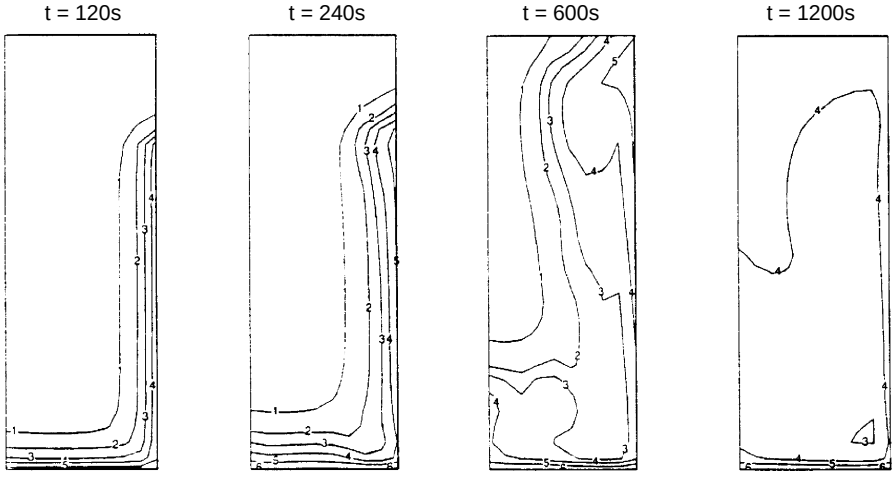

Figure 4b.
Isotherm map for bottom heating (case B)

$$Nu_H = \int_s \frac{q''H}{k_L(T_H - T_m)} ds$$

q″ is the local-heat flux, i.e., $q'' = k_L\left(\frac{\partial T}{\partial n}\right)$ and the above integral is taken over the entire surface of the fin and of the base heated wall. The results display a rapid decrease in the heat transfer rate at the early stages of melting which is

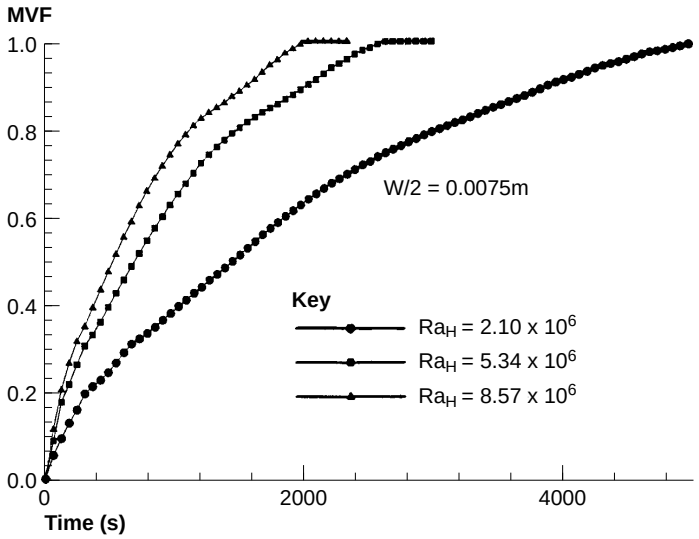

Figure 5a.
Temporal variation of the molten volume fraction for top heating (case A)

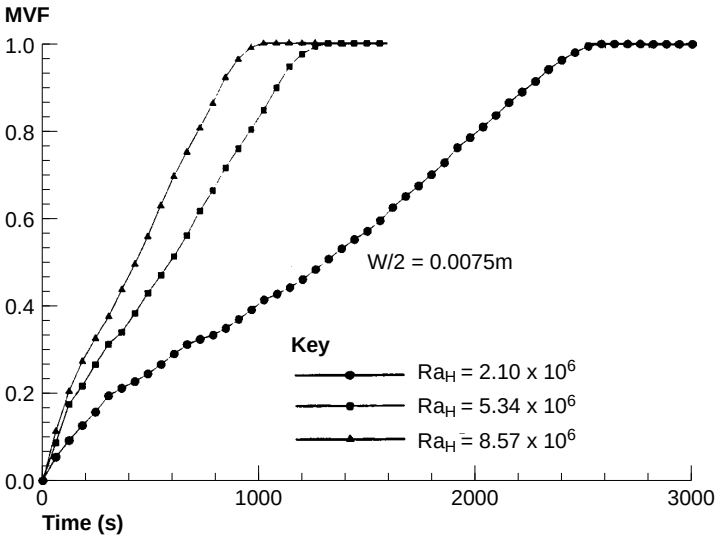

Figure 5b.
Temporal variation of the molten volume fraction for bottom heating (case B)

indicative of transient heat conduction. As melting progresses, natural convection sets in and develops, the decrease in heat transfer slows down, and then is followed by an increase over some period of time. This period of time as well as the magnitude of the increase in heat transfer depends on the Rayleigh number and on the heated surface (top or bottom). Later as the melt region becomes wider, the heat transfer coefficient passes through a local maximum

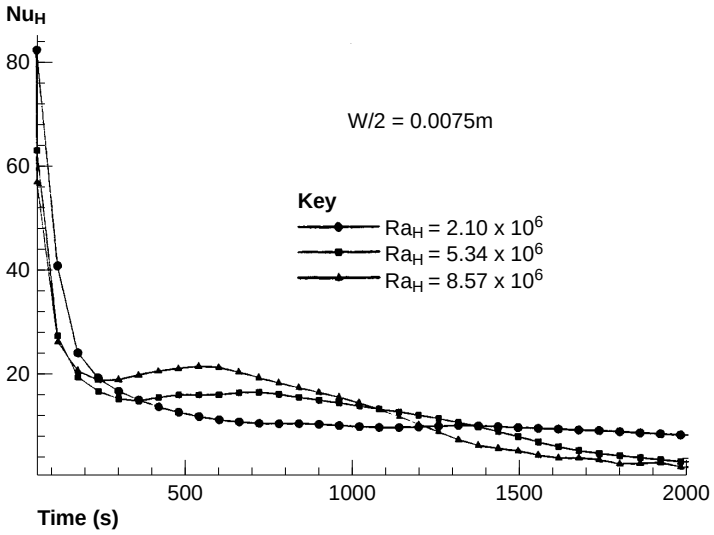

Figure 6a. Predicted average Nusselt number at the heated wall for top heating (case A)

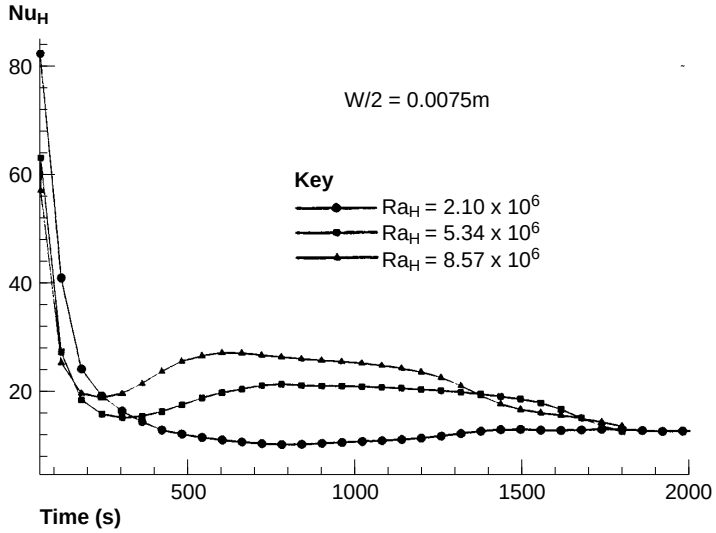

Figure 6b. Predicted average Nusselt number at the heated wall for bottom heating (case B)

and starts to decline gradually as the temperature of the melt approaches that of the heated wall.

Attention is now focused on the effect of the number of fins on the melting process. The results may best be summarized by means of the melting time with respect to the distance W (Figure 7). Scrutiny of these figures reveals that, for a given Rayleigh number, the melting time is minimized for a certain

distance between the fins. The effect is particularly evident for the bottom finned wall and the optimal distance between the fins diminishes as Ra_H increases. Indeed, as Ra_H augments, the boundary layers are thinned down and the buoyancy driven flows may develop in the increasingly restrictive space

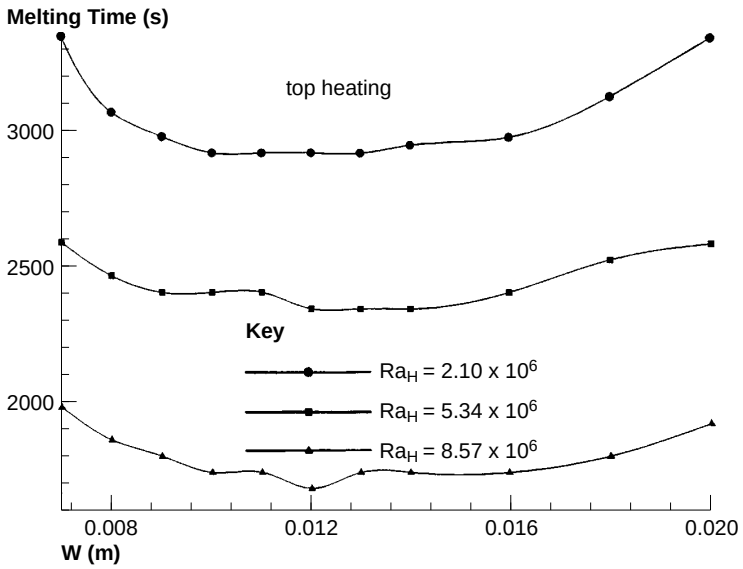

Figure 7a.
Melting time versus distance between fins; top heating (case A)

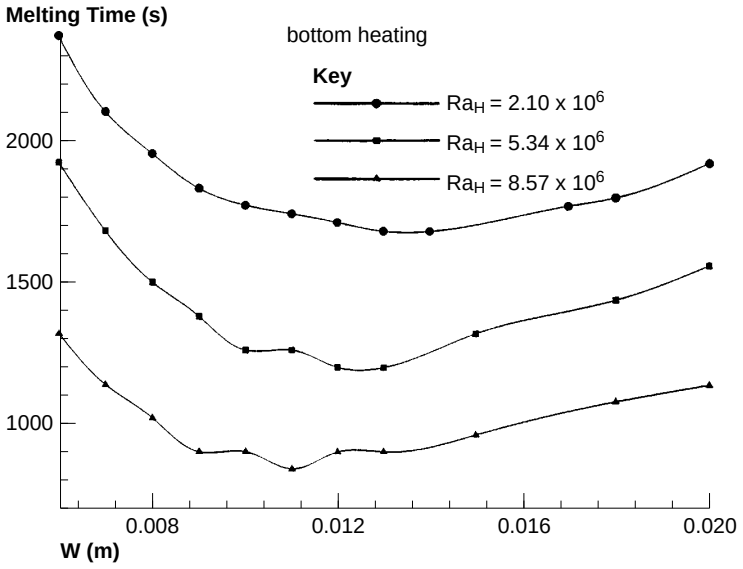

Figure 7b.
Melting time versus distance between fins; bottom heating (case B)

between the fins. Too small a distance between the fins ($W \leq 0.8$cm) prevents the onset of natural convection in the melt and the melting process is predominantly ruled by conduction heat transfer. Consequently, the melting process is slowed down, i.e. the melting time increases. Too large a distance between the fins ($W \geq 1.6$cm) reduces the total heated surface area and, as a result, the melting time augments.

The optimal distance between the fins W was correlated for the three Rayleigh numbers studied (Figure 8). The results were correlated by the following linear equation:

$$W = a\,Ra_H + b$$

where $a = -4.173 \times 10^{-8}$ and $b = 1.4376$. W is in centimeters. This correlation, which is valid for $2.10 \times 10^6 \leq Ra_H \leq 8.57 \times 10^6$, provides useful information for system design.

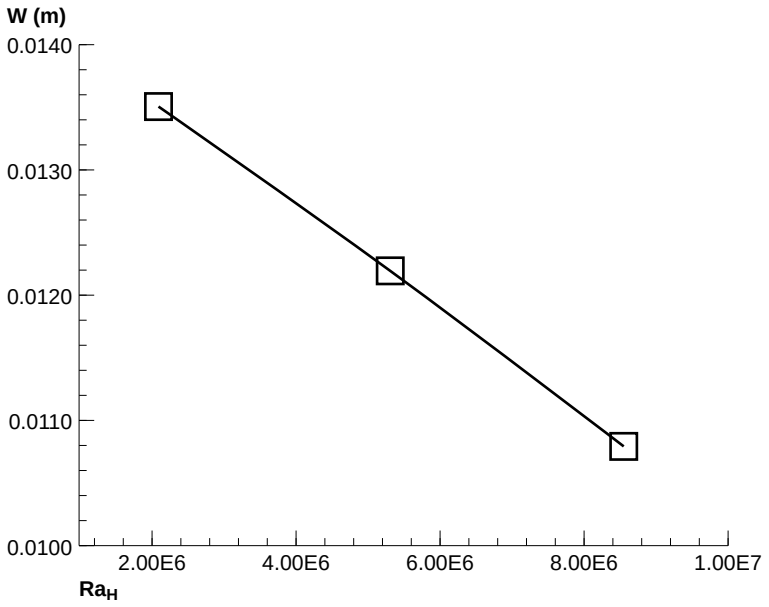

Figure 8.
Optimal distance between the fins versus the Rayleigh number

Conclusion

A numerical study has been conducted of the melting inside a rectangular horizontal enclosure with vertical fins attached to the top or to the bottom heated wall. Results have shown that melting is enhanced for a bottom finned heated wall and increasing Rayleigh numbers. It was also shown that, for a given Rayleigh number, the melting time is minimized for an optimal distance between the fins. A correlation was proposed for the optimal distance as a function of the Rayleigh number. These findings provide useful information in the improvement of the performance of latent heat thermal energy storage systems.

References

Benmadda, M. (1996), "Étude numérique de la fusion et de la solidification d'un matériau à changement de phase dans une enceinte munie d'ailettes", Thèse de doctorat (PhD), Université de Sherbrooke, Faculté des Sciences appliquées, Janvier.

Benmadda, M. and Lacroix, M. (1996), "Transient natural convection from a finned surface for thermal storage in an enclosure", *Numer. Heat Transfer, Part A,* No. 29, pp. 103-14.

Brent, A., Voller, V. and Reid, K. (1988), "Enthalpy-porosity technique for modelling convection-diffusion phase change: application to the melting of a pure metal", *Numer. Heat Transfer,* Vol. 13, pp. 297-318.

Crank, J. (1984), *Free and Moving Boundary Problems,* Clarendon Press, Oxford, UK.

Eftekhar, J., Haji-Sheikh, A. and Lou, D.Y.S. (1984), "Heat transfer enhancement in paraffin wax thermal storage system", *J. of Solar Energy Engineering,* Vol. 106, pp. 299-306.

Lacroix, M. and Benmadda, M. (1997), "Numerical simulation of natural convection-dominated melting and solidification from a finned vertical wall", *Numer. Heat Transfer, Part A,* No. 31, pp. 71-86.

Padmanabhan, P.V. and Murthy, M.V.K. (1986), "Outward phase change in a cylindrical annulus with circumferential fins", *Proceedings of the 8th Int. Heat Transfer Conference*, San Francisco, pp. 1773-9.

Patankar, S. (1980), *Numerical Heat Transfer and Fluid Flow,* Hemisphere, Washington, DC.

Sasaguchi, K. (1989), "Heat-transfer characteristics of a latent heat thermal energy storage unit with a finned tube", Trans. *JSME,* Vol. 55 No. 510, pp. 2136-43.

Sasaguchi, K. and Takeo, H. (1994), "Effect of orientation of a finned surface on the melting of frozen porous media", *Int. J. of Heat Mass Transfer,* Vol. 37 No. 1, pp. 13-26.

Sasaguchi, K., Yoshida, M. and Nakashima, S. (1988), "Heat-transfer characteristics of a latent heat thermal energy storage unit with a finned tube (effects of fin configuration)", Trans. *JSME,* Vol. 54 No. 504, pp. 2136-43.

Van Doormaal, J.P. and Raithby, G.D. (1984), "Enhancements of the simple method for predicting incompressible fluid flows", *Numerical Heat Transfer,* Vol. 7, pp. 147-63.